International Journal of Hydrogen Energy 199 (2026) 152812

Contents lists available at ScienceDirect

International Journal of Hydrogen Energy

journal homepage: www.elsevier.com/locate/he

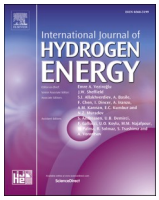

Impact of plant-derived biochars on biohydrogen production from sugar beet molasses in a continuous system: insights into the roles of microbial communities and chemical elements

Anna Detman-Ignatowska [a,**,1], Aleksandra Chojnacka [b,1], Martyna Paul [a], Gabriele Schiro [c], Jerzy Jonczak [d], Emilia Samborowska [a], Jakub Karczmarski [a], Anna Williams [c], Daniel Laubitz [c], Tadeusz Pęczek [e], Karolina Drężek [f], Anna Sikora [a,*]

[a] Institute of Biochemistry and Biophysics – Polish Academy of Sciences, Pawińskiego 5a, 02-106, Warsaw, Poland
[b] Warsaw University of Life Sciences – SGGW, Institute of Biology, Department of Biochemistry and Microbiology, Nowoursynowska 159, 02-776 Warsaw, Poland
[c] PANDA Core for Genomics and Microbiome Research, University of Arizona, 1501 N Campbell Ave, AHSC building, Room 4354. Tucson, Arizona, 85724, USA
[d] Warsaw University of Life Sciences – SGGW, Institute of Agriculture, Department of Soil Science, Nowoursynowska 159, 02-776 Warsaw, Poland
[e] Pro Civis Foundation for Education and Social Dialogue, Szkolna 36A, 25-604, Kielce, Poland
[f] Warsaw University of Technology, Chair of Drug and Cosmetics Biotechnology, Faculty of Chemistry, Noakowskiego 3, 00-664, Warsaw, Poland

ARTICLE INFO

Keywords:
Biochar
Dark fermentation
Biohydrogen
Elemental analysis
Microbial communities

ABSTRACT

Biochar shows great potential to enhance biohydrogen production via dark fermentation, but most studies have focused on short-term batch tests. This study investigates the impact of pine bark, coconut copra and cherry pit biochars in continuous bioreactors, integrating reactor performance, microbial community data, and elemental analysis. Being richest in several biologically important elements, the coconut-derived biochar produces the most significant improvement in biohydrogen yield, from 2-3 to 45 dm^3H_2/kg COD molasses. This correlates with an increased abundance of biohydrogen-producing microbial taxa and a 100-fold rise in *hydA* gene copies. Threefold-elevated butyrate and 33 %-reduced lactate levels suggest stimulation of butyrate synthesis. However, this enhancement is temporary, requiring periodic biochar replacement and bioreactor reinoculation. Although biochar promotes biofilm formation, excessive growth may inhibit activity. Furthermore, it has little influence on pH buffering but effectively adsorbs toxic metals, e.g., chromium. Overall, coconut-derived biochar is a promising but short-lived enhancer of hydrogen fermentation.

1. Introduction

Hydrogen is being called the fuel of the future, due to its high calorific value (142 kJ/g) and combustion without carbon dioxide emissions. However, conventional methods of hydrogen production create a large carbon footprint. Therefore, low- or carbon-neutral hydrogen production methods are required, of which biological methods are of particular interest. Dark fermentation, a part of acidogenesis, the second step in four-stage anaerobic digestion (AD), is considered the most promising of these. Interactions between microorganisms during AD determine which metabolic pathways are employed and consequently, the efficiency of the overall fermentation process. During acidogenesis, various acid fermentations occur, including lactic fermentations, as well as *Enterobacteriaceae*-type and *Clostridium*-type fermentations, collectively referred to as dark fermentation, where (bio) hydrogen is a key product [1–6].

The stable maintenance of efficient long-term fermentation processes is the biggest challenge when attempting to make dark fermentation a viable method of biohydrogen generation. Several well-recognized unfavorable processes can seriously inhibit biohydrogen generation during acidogenesis. These include excessive production of short-chain fatty acids (solventogenesis) or changes in the dominant fermentation type in bioreactors, especially a metabolic shift to lactic and ethanol fermentations. Throughout our research in this field, we have observed

** Corresponding author.
* Corresponding author.
E-mail addresses: annadetman@ibb.waw.pl (A. Detman-Ignatowska), annaw@ibb.waw.pl (A. Sikora).
[1] co-first authors.

https://doi.org/10.1016/j.ijhydene.2025.152812
Received 9 October 2025; Received in revised form 21 November 2025; Accepted 26 November 2025

considerable variability in the performance of bioreactors depending on the quality of the substrate, i.e., sugar beet molasses, which varies between sugar beet campaigns. The molasses can differ in the levels of specific elements, including Fe, Ca, Mg, and P, which are significant for biohydrogen production processes, and also in the content of reducing compounds (unpublished internal reports). It has recently been shown that the production of biohydrogen, short-chain fatty acids, and alcohols during dark fermentation can be controlled by redox mediators, which alter the redox potential and electron transfer between enzymatic complexes, directing NADH towards reactions leading to biohydrogen formation instead of solventogenesis [7–11].

Recently, much attention has been focused on the enrichment of substrates with various additives that stimulate dark fermentation and enhance biohydrogen production, e.g., metals and metal compounds to increase electron flow, compounds ensuring an appropriate redox potential (L-cysteine) or those such as biochar and cross-linking polymers that promote the immobilization of microorganisms [12–15].

Biochar is a solid carbon material, the precursor to activated carbon, that is obtained by thermochemical conversion of biomass or other organic materials under anaerobic conditions. Its chemical composition and structure are determined by the starting material and pyrolysis conditions, including the maximum temperature and heating gradient, time of pyrolysis, and the extraction of oils [16,17]. Initially, biochar was shown to have a positive impact on biogas (biomethane) production [18,19]. In recent years, numerous studies have reported the positive effects of biochar on biohydrogen production efficiency during dark fermentation, attributing the improvements to the following mechanisms: (i) stimulating or mediating electron transport within microbial communities; (ii) lowering the redox potential; (iii) providing buffering capacity; (iv) enhancing the immobilization of bacterial biofilms; (v) adsorbing inhibitory compounds, and (vi) releasing beneficial micronutrients or mineral compounds. It is worth emphasizing that one of the most crucial mechanisms of biochar action may involve extracellular electron transfer, primarily by serving as an electron shuttle, but also possibly by enabling direct physical connections between electroactive microorganisms, although this requires further investigation [13,16,20,21].

However, nearly all studies on the effect of biochar on biohydrogen production during dark fermentation have been conducted in short-lived batch fermentation systems with small total volumes (50–200 mL). In some of these, the biochar was enriched with metals such as iron or nickel, resulting in a synergistic effect on biohydrogen yield [22–31].

Industrial-scale processes are typically long-term operations conducted in continuous or quasi-continuous systems, so for commercial viability, short-term static (batch) fermentations require further optimization in dynamic flow systems and adaptation to the operational scale. Therefore, in the present study, we used a long-term continuous system to examine the influence of three different biochars (from pine bark, coconut copra and cherry pits) on the efficiency of biohydrogen production via dark fermentation. The poor performance observed in the control reactor (without biochar) indicated that the system operated under unfavorable conditions for biohydrogen production. Consequently, the main objective of this study was to assess whether the addition of biochar could overcome these conditions and improve biohydrogen yields. We found that biochar derived from coconut copra was the most effective in counteracting the extremely unfavorable background for dark fermentation. Analysis of the metabolic potential of the microbial communities using digital PCR (dPCR) revealed a significant overrepresentation of genes encoding hydrogenases in the bioreactors with coconut copra. This noteworthy discovery adds to our understanding of the mechanisms of biochar action on biohydrogen-yielding processes. Interestingly, we observed exhaustion of the beneficial properties of biochar. Our findings are discussed in the context of microbial community dynamics, microbial metabolites, and the elemental composition of biochar.

2. Materials and methods

2.1. Biochar preparation

The biochars were produced and made available by InnEco Sp. z o.o. (Poland). They were prepared from waste materials remaining after coconut oil production (designated as K), cherry pits (W), and pine bark (S). Pyrolysis of each material was carried out in two ways. In the first procedure (B1), slow low-temperature pyrolysis with oil extraction was performed. The maximum temperature was 450 °C, the time to reach this temperature was 72 h, the duration of maximum temperature maintenance was 2 h, and oil extraction (distillation) occurred during this process. The second procedure (B3) involved rapid high-temperature pyrolysis without oil extraction. The maximum temperature was 650 °C, the time to reach this temperature was 6 h, and the maximum temperature maintenance time was 2 h. The initial biochar material was mechanically fragmented using a standard milling procedure and sieved through a 5-mm mesh to obtain a uniform particle size ($\leq$5 mm), minimizing variability in surface area and ensuring consistent physical properties. A total of six biochar preparations were used in the study, named according to the specific starting material and preparation method employed: KB1, KB3, WB1, WB3, SB1 and SB3.

The SB biochars had pH values of 6.77 (SB1) and 6.36 (SB3) with ash contents of 1.5 % and 2.6 %, respectively; the WB biochars had pH values of 4.95 (WB1) and 7.59 (WB3) with ash contents of 1.7 % and 2.4 %; whereas the KB biochars showed the highest pH values of 10.46 (KB1) and 10.45 (KB3), along with the highest ash contents of 4.1 % and 9.2 %, respectively.

2.2. Experimental set-up

Seven 3-L plexiglass PBRs, packed-bed bioreactors, (KB1, KB3, WB1, WB3, SB1, SB3, and C–control without biochar) were filled with sterilized 15-mm ceramic Raschig rings (2-L working volume), 75 g of the respective biochar, and M9 medium [32] supplemented with sugar beet molasses from the Dobrzelin Sugar Factory (Poland) at 32 g COD (chemical oxygen demand)/L. The bioreactor design was as described by Chojnacka et al. [33], except that Raschig rings replaced granite stones. The inoculum was the microbial community from a previously described underperforming PBR [34].

After inoculation, all bioreactors were incubated at room temperature (21–25 °C) for 7 days. From day 7 onward, fresh medium was continuously supplied via a peristaltic pump (ZALIMP, Poland), with a hydraulic retention time of 12–24 h (see Supplementary Table 1). Bioreactors SB1, SB3, WB1 and WB3 operated for 29 days, while KB1, KB3 and the control (C) ran for 43 days. In an additional test (days 29–43), biochar KB3 was added to the control (C) reactor on day 32. A detailed record of the bioreactors' operation is presented in Fig. 1.

2.3. Analytical methods

The total rate of fermentation gas production from the bioreactors was measured (10 measurements for each time point, for each bioreactor) using a bubble flowmeter (Zakłady Urządzeń Przemysłowych ZAM Kęty, Poland). In each case, a mean ± SD (standard deviation) was calculated. The composition of the fermentation gas was analyzed using an HPR20 mass spectrometer (Hiden, England) with QGA software version 1.37.

The pH of the media and the effluents from the bioreactors was measured using a standard pH meter (ELMETRON, model CP-502, Poland) equipped with a combination ORP (redox, mV) electrode type ERPt-13. The chemical oxygen demand (COD) was determined using a NANOCOLOR COD 1500 kit (Machery-Nagel) according to ISO 1575:2002.

Metabolite concentrations were quantified by GC/MS using a Trace 1310 GC System (Thermo Scientific) coupled to a TSQ9000 Triple

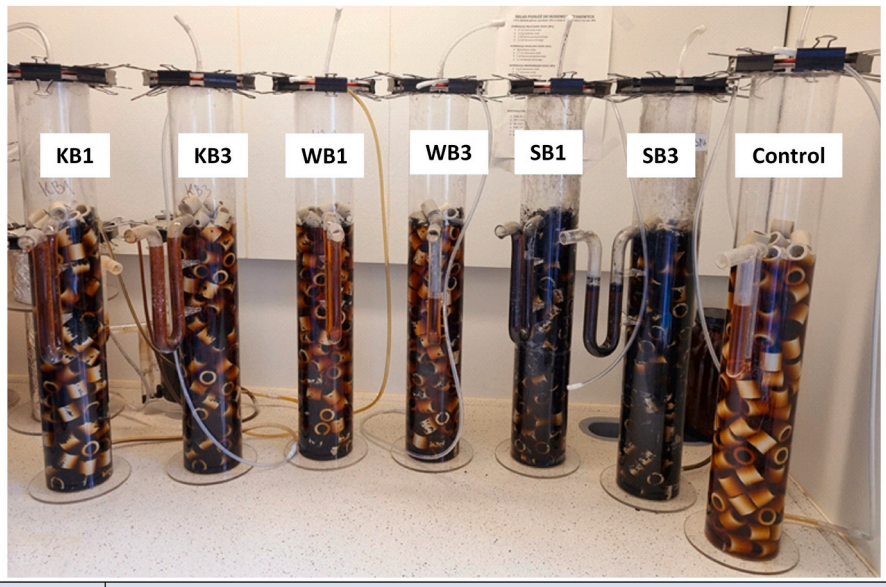

Days of bioreactor operation	Actions	
STAGE I: operation of 7 bioreactors		
1-7	inoculation and propagation	Inoculation of seven bioreactors (SB1, SB3, WB1, WB3, KB1, KB3 and control), incubation in stationary conditions for bacteria propagation
8-14	phase 1	Supply of media to all bioreactors, continuous operation of the bioreactors
15	renewal 1	Renewal of the cultures in all bioreactors by removal of excess biomass
16-21	phase 2	Supply of media to all bioreactors, continuous operation of the bioreactors
22	renewal 2	Renewal of the cultures in all bioreactors by removal of excess biomass and reinoculation (using the same inoculum as at the beginning of the experiment)
24-29	phase 3	Supply of media to all bioreactors, continuous operation of the bioreactors
29		End of experiment for bioreactors WB1, WB3 and SB1 and SB3.
STAGE II: operation of 3 bioreactors		
32	renewal A	Renewal of the cultures in bioreactors KB1, KB3 and control (C) by removal of excess biomass. Adding KB3 biochar to bioreactor C.
33-36	phase A	Supply of media to all bioreactors, continuous operation of the bioreactors
36	renewal B	Renewal of the cultures in all three bioreactors by removal of excess biomass, adding KB3 biochar to the control bioreactor and reinoculation (using the same inoculum as at the beginning of the experiment)
37-43	phase B	Supply of media to all bioreactors, continuous operation of the bioreactors
43		End of the experiment
Analyses- day of sampling		
Biochar	Elements: 15^{th}, 22^{nd}, 29^{th} (except KB1 and KB3), 43^{rd} (only KB1 and KB3) Microscopic: 29th	
Effluents	Elements: 12^{th}, 22^{nd}, 26^{th} (except KB1 and KB3), 29^{th} GC/MS: 12^{th}, 22^{nd}, 26^{th} (only KB1 and KB3), 29^{th}	
Microbial community	16S rRNA amplicon sequencing: 12^{th}, 22^{nd}, 26^{th} (only KB1 and KB3), 29^{th}	

Fig. 1. Experimental set-up and record of the bioreactors' operation.

Quadrupole mass spectrometer (Thermo Scientific). Chromeleon 7 software was used for instrument control and data acquisition. MS data were collected in Selected Reaction Monitoring mode. The respective calibration curves and internal standards were used. Short-chain fatty acids (SCFA) analysis was performed using the analytical method described by Ostrowska et al. [35]. Ethanol concentration was determined according to the method of Pinu & Villas-Boas [36]. The derivatization of γ-aminobutyric acid (GABA) was performed based on the protocol of Sun et al. with slight modifications [37]. DB-1701 and TG-5SilMS columns were used for chromatographic separations.

2.4. Elemental analysis of biochars and effluents

Biochar samples were milled into a fine powder for chemical analysis. Their pH was determined potentiometrically in a water suspension at a biochar-to-water ratio of 1:10. The total contents of carbon (C),

nitrogen (N) and sulfur (S) were determined by dry combustion using a Vario MacroCube analyzer (Elementar, Germany). The concentrations of phosphorus (P), sodium (Na), potassium (K), calcium (Ca), magnesium (Mg), iron (Fe), aluminum (Al), manganese (Mn), copper (Cu), zinc (Zn), nickel (Ni), lead (Pb), chromium (Cr), vanadium (V), strontium (Sr), barium (Ba), titanium (Ti) and zirconium (Zr) were determined using inductively coupled plasma atomic emission spectrometry (ICP-AES, Avio 200, PerkinElmer, USA), following microwave-assisted digestion (Ethos Up, Milestone, Italy) with a mixture of 65 % HNO_3 and 38 % HCl in a 3:1 vol ratio.

The aforementioned elements were also quantified in the bioreactor effluents using the same analytical techniques and instrumentation. The only difference was the digestion method, in which 65 % HNO_3 alone was used. Only reagents of analytical grade purity were used. Certified reference materials were employed to ensure data quality and analytical accuracy.

2.5. Scanning electron microscopy

Initial and post-experimental biochars were analyzed using a FEI Quanta 200 Environmental Scanning Electron Microscope (ESEM). Samples were mounted on stubs with carbon tape and examined under low vacuum conditions without gold coating. Imaging was conducted at a chamber vacuum of 0.98–1.00 Torr, temperature of 1 °C, and relative humidity of approximately 20 %. These conditions permitted the observation of surface morphology without extensive sample preparation. SEM images were used to identify structural differences between untreated and treated biochars.

2.6. Microbial DNA extraction and 16S rRNA amplicon sequencing and data analysis

Two 15-ml samples (duplicates) containing microbial biofilm suspended in the fluid phase were collected from the inner middle part of the bioreactors on the following days of the experiment: 12, 22 and 29 for each bioreactor, and additionally on day 26 for KB1 and KB3. The samples collected for microbial community analysis included both the fluid phase containing flocks and granules, as well as the bacterial biofilms formed on the surfaces of Raschig rings and biochars. Total DNA was isolated from 250 to 300 mg of material pelleted by centrifugation of the duplicate samples. DNA was extracted and purified using a DNeasy PowerSoil Pro Kit (Qiagen, Cat. No. 47014) according to the manufacturer's protocol. Cell lysis was achieved using a Vortex-Genie 2 equipped with a Vortex Adapter for 1.5–2 ml tubes (Cat. No. 13000-V1-24). The preparations of DNA isolated from the duplicate samples were pooled and stored at −20 °C. Extraction blanks were included for contamination control during extraction and sequencing.

The V4 hypervariable region of the 16S rRNA gene was PCR-amplified using the primer pair 515-F and 806-R [38], which carried Illumina adapters and a unique 12-nt barcode for each sample. The PCR products were quantified with a Quant-iT PicoGreen dsDNA iAssay Kit (Invitrogen). DNA amplicons from each reaction were then pooled in equimolar concentrations, and fragments longer than 200 bp were selected using QIAseq beads and sequenced on a 2x150 bp Illumina MiSeq platform (Illumina) at the PANDA Core for Genomics and Microbiome Research, University of Arizona, USA. Demultiplexing was performed using idemp (https://github.com/yhwu/idemp). The DADA2 pipeline was used to infer amplicon sequence variants (ASVs). The reads were trimmed to 145 bp, and low-quality reads exceeding a maximum expected error of 2 bp were removed. The resulting quality-filtered reads were used to train the error model in DADA2. Paired-end reads were merged and chimera sequences eliminated. Taxonomic identities were assigned using the Ribosomal Database Project (RDP) classifier [39] on the SILVA nr version 138.1 database [40]. The number of reads per sample after quality filtering, error correction, chimera removal and taxonomy cleaning ranged from 47,552 to 103,732. Reads were rarefied to a depth of 47,000 for further analysis. The raw sequences generated in this study have been deposited in the NCBI databases with the BioProject accession number PRJNA1291707, submission ID SUB15462781.

Principal component analysis (PCA) was conducted using GraphPad Prism (version 10.4.0621). A total of 73 variables were included in the dimensionality reduction process. To improve the interpretability of the multivariate structure, the loading plot displays the top 30 vectors, which represent variables with the strongest contributions to the first principal components. This method allowed the identification of the most influential parameters driving sample separation while maintaining the overall variance structure of the dataset. Data used for the analysis are provided in Supplementary Table 3.

2.7. Digital PCR (dPCR)

Quantification of the *hydA* gene was performed using the QIAcuity Digital PCR System (QIAGEN) with a QIAcuity Nanoplate 8.5k. Each 10 μL reaction mixture consisted of 1 μL of a *hydA*-specific primer set (forward: 5′-AAGAAGCTTTAGAAGATCCTAA-3′; reverse: 5′-GGACAA-CATGAGGTAAACATTG-3′) [41], 4 μL of QIAGEN EvaGreen Supermix, 3 μL of nuclease-free water, and 2 μL of template DNA (2 ng/sample). Thermal cycling was performed with an initial denaturation step at 95 °C for 5 min, followed by 40 cycles of 57 °C for 45 s for annealing and elongation. Fluorescence was read post-PCR using FAM channels, and the data were analyzed with the QIAcuity software suite using default thresholds and Poisson statistical modeling to calculate absolute quantification. No template controls (NTC) were run in triplicate on each plate. Data were excluded if NTCs exhibited a signal above baseline or if partition fill was below 85 %.

2.8. Statistics

The collected data were statistically analyzed to identify differences among group means. Analysis of variance (ANOVA) was employed as the primary statistical method, followed by Tukey's post hoc test to assess pairwise comparisons. A significance threshold of $p < 0.05$ was applied to determine statistically significant differences. Analyses were performed using GraphPad Prism software, Version 10.4.10 (GraphPad Software, San Diego, CA, USA), and Microsoft Excel (Microsoft Office LTSC Professional Plus 2021). Venn network diagrams were generated using the EVenn platform [30].

3. Results and discussion

3.1. Effects of biochars on biohydrogen production via dark fermentation

The effect of three biochars (from coconut copra [KB1, KB3], cherry pits [WB1, WB3], and pine bark [SB1, SB3]) on biohydrogen production via dark fermentation was studied in seven continuous PBRs fed with molasses. Based on the poor performance of the control reactor (without biochar), it was inferred that the system operated under unfavorable conditions for biohydrogen production.

The experiment was conducted in two stages: stage I (days 1–29) with all reactors in operation, and stage II (days 30–43), during which only KB1, KB3 and the control (C) remained active. On day 32, fresh KB3 biochar was added to reactor C (Fig. 1). In stage I, after inoculation and propagation, the following phases were distinguished: continuous operation phase 1, renewal 1, continuous operation phase 2, renewal 2, and continuous operation phase 3. Continuous operation phase 1 demonstrated the positive and varied impact of the tested biochars on biohydrogen production. The yield of 3.2 dm^3 $bioH_2$/kg COD molasses from reactor C was much lower than the yields of 25.4, 23.2, 20.4, 42.7, 14.4 and 22.4 dm^3 $bioH_2$/kg COD molasses from reactors KB1, KB3, SB1, SB3, WB1 and WB3, respectively. In terms of their positive effect on biohydrogen production, the tested biochars were ranked as follows: SB3>KB1>KB3>WB3>SB1>WB1, with the strongest stimulating

properties observed for pine bark biochar prepared using method B3, and the weakest for cherry pit biochar prepared using method B1 (Fig. 2A).

After renewal 1, which involved removing excessive bacterial biomass, continuous operation phase 2 occurred, during which the efficiency of biohydrogen production was unexpectedly low: <2 dm^3 bio-H_2/kg COD molasses in all bioreactors. During renewal 2, biochar replacement and reinoculation were performed in addition to removing excess bacterial biomass. In continuous operation phase 3, the strongest stimulating effect on biohydrogen production was observed for coconut copra biochars, with yields of 45.0 and 50.4 dm^3 bioH_2/kg COD molasses for KB1 and KB3, respectively. The performance of biochar WB3 remained unchanged, while surprisingly, no stimulation was observed with the SB3, WB3 or SB1 biochars (<5 dm^3 bioH_2/kg COD molasses) (Fig. 2B). The ranking of biochars based on their stimulating effect was as follows: KB3>KB1>WB3>SB3≈SB1≈WB1. The performance of the control bioreactor remained unchanged. Among the biochars, those derived from pine exhibited the highest brittleness. Their initial distribution within the bioreactor was uniform; however, following subsequent renewals, they tended to fragment and settle towards the bottom of the bioreactor to form compacted structures. Notably, these biochars generated the largest amount of fine particulate matter, which was washed out from the bioreactor along with the post-fermentation effluent during the bioreactor's operation.

The second stage of the experiment, stage II (days 30–43), was divided into four phases: renewal A, continuous operation phase A, renewal B, and continuous operation phase B. Renewal A involved the removal of excess bacterial biomass from bioreactors KB1, KB3 and C, as well as the addition of fresh KB3 biochar to the control bioreactor C. During continuous operation phase A an unexpectedly low efficiency of biohydrogen production was observed, not exceeding 5 dm^3 bio-H_2/kg COD molasses in reactors KB1 and KB3. Renewal B was analogous to renewal 2 of stage I, and involved the removal of excess bacterial biomass, reinoculation and biochar replacement in reactors KB1, KB3 and C, with fresh KB3 biochar being added to C. In continuous operation phase B, biohydrogen yields were comparable across all bioreactors, averaging 45.3, 40.4 and 42.5 dm^3 bioH_2/kg COD molasses for bioreactors C, KB1 and KB3, respectively (Fig. 2C). These results were similar to the performance of bioreactors KB1 and KB3 in the third continuous operation phase of stage I. Stage II was a proof-of-concept experiment demonstrating the strong stimulating effect of copra coconut-derived biochar on biohydrogen production and the reproducibility of this phenomenon. The average yield obtained in bioreactor C after supplementation with KB3 biochar increased approximately 15-fold compared to the yield without biochar addition. Both stages of the experiment also demonstrated the occurrence of exhaustion of biohydrogen production stimulation by the biochars over time, since following renewals involving only the removal of excess biomass, the performance of biochar-enhanced bioreactors did not differ from the control. Strong evidence for this phenomenon is provided by the coconut copra-derived biochars in reactors KB1 and KB3. Another key factor here is the addition of new inoculum (reinoculation). The issue of the exhaustion (depletion) of biochar and the need for reinoculation is further examined in section 3.5.

Bioreactor performance was unaffected by the pyrolysis temperature (B1 vs. B3) but varied significantly with the type of biomass used for biochar production, as observed in previous studies [21]. Moreover, other reports have confirmed the positive effect of coconut-derived biochar on biohydrogen production [42,43].

In the continuous system presented here, the increase in biohydrogen production is consistent with the mechanisms reported for batch tests. However, the stimulatory effect was transient and declined during prolonged operation, which cannot be observed in batch systems.

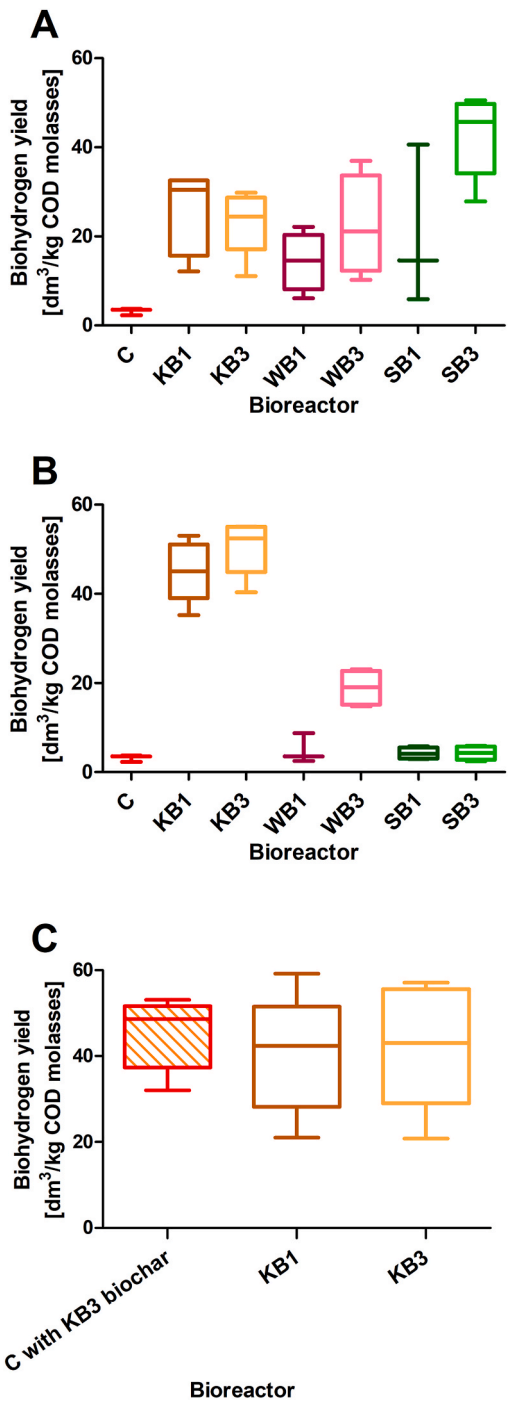

Fig. 2. Efficiency of biohydrogen production in bioreactors throughout their operation: A. Stage I, continuous operation phase 1 (days 8–14). Statistically significant differences (Tukey's Multiple Comparison Test) were observed for C vs. SB3 (***) and WB1 vs. SB3 (**); B. Stage I, continuous operation phase 3 (days 24–29). Statistically significant differences (Tukey's Multiple Comparison Test, $p < 0.05$) were observed for C vs. KB1 (***), C vs. KB3 (***), C vs. WB3 (**); KB1 vs. WB1 (***), KB1 vs. WB3 (***), KB1 vs. SB1 (***), KB1 vs. SB3 (***); KB3 vs. WB1 (***), KB3 vs. WB3 (***), KB3 vs. SB1 (***), KB3 vs. SB3 (***); WB1 vs. WB3 (**); WB3 vs. SB1 (**) and WB3 vs. SB3 (**). C. Stage II, continuous operation phase B (days 37–43); no statistical differences were observed. The lower and upper sides of each box represent the first and third quartiles, respectively. The whiskers extend to the minimum and maximum values, while the middle line indicates the median value. *$p < 0.05$; **$p < 0.01$; ***$p < 0.001$.

3.2. Effects of biochars on non-gaseous fermentation products

Metabolic processes in bioreactors are reflected not only in the composition of the fermentation gas, but also in the characteristics of the effluent containing non-gaseous fermentation products.

The effluent pH ranged from 4.0 to 4.7, which is typical for acidic fermentations, with some significant differences observed between reactors (Fig. 3 and Supplementary Table 1). During stage I, a significantly higher pH was observed in reactor SB3 during phase 1, characterized by high biohydrogen production, compared to phase 3, where biohydrogen production was lower ($p < 0.01$). However, in stage II, the pH of effluents from high-performing biohydrogen-producing reactors KB1 and KB3 was lower than that of the poorly performing control reactor in stage I (KB1 stage II vs. C stage I, $p < 0.001$; KB3 stage II vs. C stage I, $p < 0.01$). The finding that pH values in biochar-containing reactors were either lower or unchanged compared to the control was unexpected, considering that the optimal pH for biohydrogen production is approximately 5 [44–46]. With the exception of a few studies [22,24,31], biochar is generally reported to buffer the fermentation environment. This buffering capacity is associated with its surface functional groups and mineral ash content [16,19,21]. In our experiments, the biochars displayed considerable variation in both pH and ash content (Section 2.1), with the highest pH values (exceeding 10) and the highest ash content observed for KB, the strongest stimulator of biohydrogen production. Although the final pH of the effluent remained unchanged, local pH variations may occur in the bioreactors, particularly in specific niches near the biochar surface, especially KB. Future study of this phenomenon is warranted.

Metabolite concentrations in the effluents were analyzed only during stage I on days 12, 22 and 29, except for reactors KB1 and KB3, which were sampled on day 26 instead of day 29. Averaged stage I results showed no significant differences between bioreactors, probably due to operational instability and high data variability (Supplementary Fig. 1 and Supplementary Table 1). However, certain trends can be observed in relation to biohydrogen production on specific days (Fig. 4).

Generally, lactic acid was the main effluent component, with the highest average concentrations of about 10–11 g/L in bioreactors WB1, SB1 and SB3, followed by WB3, C and KB1 with around 9 g/L (Supplementary Fig. 1 and Supplementary Table 1), indicating that fermentations unfavorable for biohydrogen production were co-occurring in the bioreactors. Notably, the lowest lactic acid concentrations of <6 g/L were observed in the bioreactors with coconut copra biochar during the most efficient biohydrogen production periods (day 26 for KB1, and days 12 and 26 for KB3), as shown in Fig. 4 and Supplementary Table 1. This is consistent with the observation that the acetate concentration was lowest in bioreactors KB1, KB3 and SB3, which showed the highest biohydrogen production. It is well recognized that in conditions optimal for the production of biohydrogen, lactic acid is a minor product because, together with acetic acid, it is converted into butyric acid, a relevant metabolic pathway in biohydrogen production [34,44–47]. The butyrate level was highest in the bioreactors supplemented with coconut copra biochar, with average concentrations of 3.0 g/L for KB1 and 2.9 g/L for KB3 (Supplementary Fig. 1 and Supplementary Table 1). It is noteworthy that during the continuous operation phase 1 (day 12) and phase 3 (day 26), characterized by high biohydrogen production, the butyrate concentration was markedly elevated compared to the end of phase 2 (day 22), when a low yield of biohydrogen was observed. This was particularly striking in bioreactor KB3, where the difference was over 10-fold (Fig. 4, Supplementary Table 1). The average butyrate concentration in bioreactors SB3, WB1 and WB3 was about 1 g/L (Supplementary Fig. 1). However, in SB3 on day 12, at the end of continuous operation phase 1, it reached 3.3 g/L, and this bioreactor exhibited the highest biohydrogen production efficiency during that phase (Fig. 4, Supplementary Table 1). The lowest butyrate concentrations of <0.1 g/L were found in bioreactors SB1 and C. Notably, a low concentration of butyrate in dark fermentation bioreactors is always associated with low biohydrogen production efficiency [34,44–48].

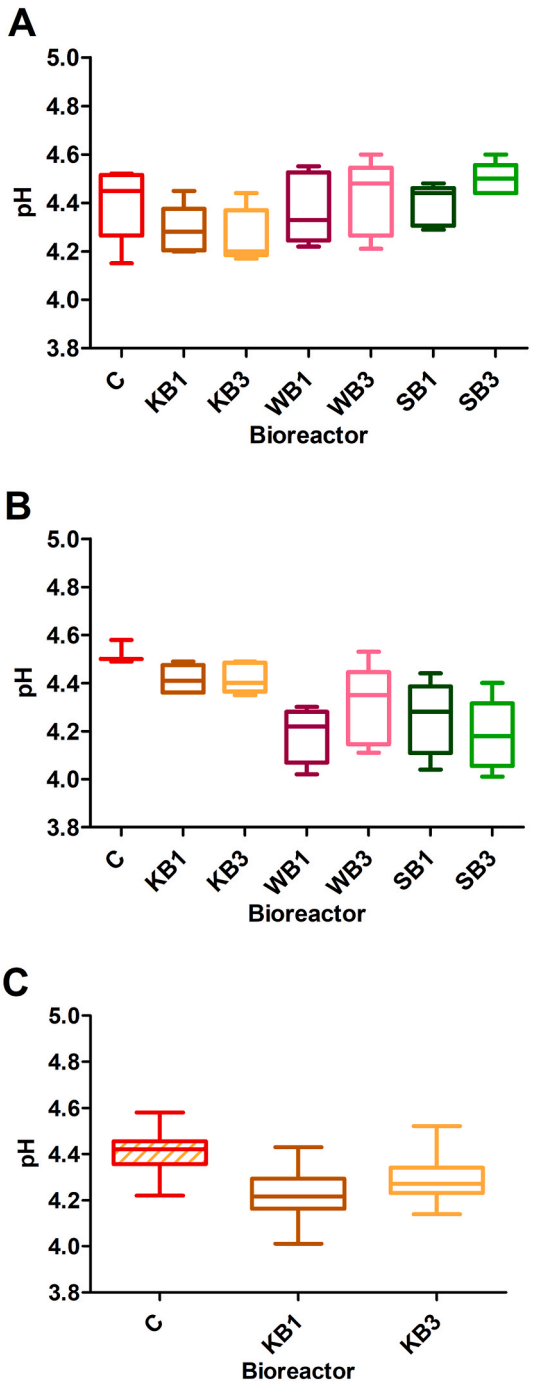

Fig. 3. pH of effluents from the bioreactors: A. Stage I, continuous operation phase 1 (days 8–14). No statistically significant differences were observed; B. Stage I, continuous operation phase 3 (days 24–29). Statistically significant differences (Tukey's Multiple Comparison Test) were observed for C vs. SB1 (*) and C vs. SB3 (*); C. Stage II, continuous operation phase B (days 37–43). Statistically significant differences (Tukey's Multiple Comparison Test, $p < 0.05$) were observed for C vs. KB1 (*). The lower and upper sides of each box represent the first and third quartiles, respectively. The whiskers extend to the minimum and maximum values, while the middle line indicates the median value. *$p < 0.05$; **$p < 0.01$; ***$p < 0.001$.

The presence of propionate and ethanol among the fermentation products in dark fermentation bioreactors is also undesirable, because it is indicative of solventogenesis. Interestingly, ethanol concentrations

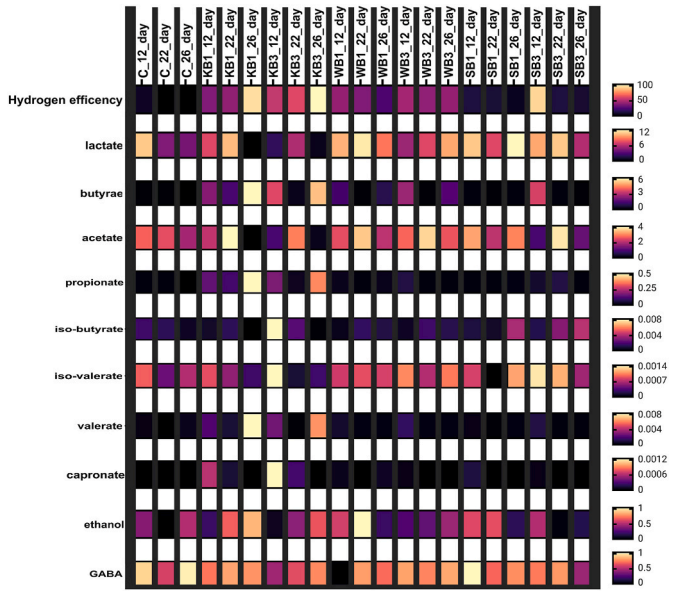

Fig. 4. Non-gaseous fermentation products (g/L) in the effluents from the bioreactors in stage I. The measurements were taken on days 12, 22, and 29, except for reactors KB1 and KB3, which were sampled on day 26 instead of day 29. The upper row shows biohydrogen production yield on individual days, expressed in dm^3/kg of COD from sugar beet molasses. Each metabolite concentration for individual days, shown in the heatmap (Fig. 4), is based on two determinations.

were higher in all bioreactors supplemented with biochars produced using method B1 (0.4–0.5 g/L) compared to those using method B3 and the control (0.2–0.3 g/L), which indicates that oil extraction from biochar feedstock impacts the course of ethanol fermentation. The levels of other minor metabolites, such as caproate, 2-methyl butyrate and valerate were low (<0.1 g/L) and similar across all bioreactors (Supplementary Fig. 1 and Supplementary Table 1).

3.3. Effect of biochars on microbial community dynamics

The performance of bioreactors and the processes occurring within them are governed by the microbial communities they contain. Samples for microbial community analysis were collected from the bioreactors at the sampling time points for metabolite and biochar analyses at the end of continuous operation phases 1 and 3 in stage I. The taxonomic composition of these communities was then determined by sequencing the V4 region of 16S rRNA amplicons.

Comparative analysis of microbial diversity shows statistically similar richness (denoted by the letter "a" above the boxes), indicating no significant differences between any biochar or the control (Fig. 5A). Major bacteria (>1 % of the microbial community) include genera such as *Escherichia-Shigella*, *Serratia*, *Leuconostoc*, *Lactoplantibacillus, Fructobacillus*, *Liquorilactobacillus*, *Lentilactobacillus* and others (Fig. 5B, upper panel). Minor bacteria (<1 % of the microbial community) include genera such as *Clostridium sensu stricto, Lacticaseibacillus, Caproiciproducens, Prevotella, Eubacterium* and others (Fig. 5B, lower panel). Fig. 5B highlights the dynamic changes in community structure depending on the biochar and time. For the detailed taxonomic assignments, see Supplementary Table 2. The heatmap (Fig. 5C) shows variation in the abundance of the selected *Clostridium sensu stricto* subgroups (1, 11, 12 and 16) across biochars and time points. Notably, a higher abundance of *Clostridium sensu stricto 1* is observed in KB1 and KB3, which exhibit high biohydrogen production. The microbial co-occurrence network (Fig. 5D) highlights associations between specific bacterial genera and particular biochar types, clustering bacterial communities associated with different biochar types. For example, genera such as *Prevotella* 7, *Eubacterium* and *Clostridium sensu stricto* 12 appear to be closely associated with bioreactor KB3 (biochar associated with higher biohydrogen production). In our previous studies, *Clostridium sensu stricto* subgroups 11 and 12, as well as *Prevotella* and *Caproiciproducens*, were identified as dominant taxa in continuously operating dark fermentation bioreactors with high biohydrogen production efficiency [34], as well as in stationary batch cultures [44]. These systems were maintained under conditions favorable for the conversion of lactate and acetate to butyrate, a key metabolic pathway for biohydrogen production in bacterial communities. In contrast, we did not observe a positive correlation between *Clostridium sensu stricto* 1 and biohydrogen production [44,49], although other reports indicate that this taxon is found in bioreactors with high biohydrogen yields [50].

3.4. Effect of biochars on the metabolic potential of microbial communities

To evaluate the effect of biochars on the biohydrogen production potential of microbial communities, the abundance of the *hydA* gene encoding hydrogenase I was quantified using digital PCR (dPCR) (Fig. 6A). [FeFe]-hydrogenase I, a key enzyme in biohydrogen production, is the most well-studied hydrogenase [41,51–53]. Several groups have examined the expression of the *hydA* gene while determining the impact of various factors on biohydrogen production to assist subsequent process optimization. In previous studies, quantitative PCR (qPCR) was used to examine *hydA* gene copy number and reverse transcription-quantitative PCR (RT-qPCR) was used to quantify *hydA* mRNA expression in response to various factors in pure strains of *C. butyricum* [41,53], in individual isolates from dark fermentation communities [51], and in entire microbial consortia grown in stationary batch cultures. In this study, we employed dPCR to determine the *hydA* gene copy number in total DNA extracted from microbial communities selected in the bioreactors. This approach, which assesses metabolic potential based on *hydA* gene abundance, appears to be a novel application of this technique in the analysis of microbial communities in continuously operating bioreactors.

Our dPCR analysis revealed variations in the presence of the hydrogenase gene, indicating that biochars had a differential impact on *hydA* gene abundance within the microbial consortia (Fig. 6A). Specifically, the coconut copra-derived biochar significantly increased hydrogenase gene abundance from an average value of 12.2 copies/μl in the control bioreactor to median values 2245 copies/μl in KB1 and 1380 copies/μl in KB3, highlighting its role in enhancing microbial hydrogen production activity. A similar, albeit weaker effect was observed with pine bark-derived biochar in the SB3 bioreactor during the end of phase 1, stage I (230 copies/μl), coinciding with the highest biohydrogen production levels. At the end of phases 2 and 3 of stage I, the number of copies decreased to ~83 per μl. The average values for WB1 and WB3 were comparable, at ~41 copies/μl, whereas for SB1, the value was 28.3 copies/μl.

The dPCR data revealed that biochar-induced modulation of microbial hydrogen production coincided with an increased number of bacteria carrying hydrogenase genes. The abundance of the *hydA* gene, together with other biohydrogen-related indicators, biohydrogen production efficiency and biohydrogen content, was used for correlation analysis with microbial community profiles to elucidate the functional role of specific hydrogen-yielding bacterial genera (Fig. 6B). Among the major bacterial genera, *Liquorilactobacillus* and *Klebsiella* show the strongest positive correlations with biohydrogen production parameters, while among the minor genera, *Clostridium sensu stricto* 1, *Clostridium sensu stricto* 12 and *Prevotella* are also positively associated. Conversely, major genera such as *Lactiplantibacillus* and *Lentilactobacillus*, as well as minor genera including *Lacticaseibacillus* and Subgroup 10, exhibit negative correlations with biohydrogen yield and *hydA* gene abundance. These correlations are consistent with the results presented in Fig. 5C and D, especially in relation to the minor genera. Members of

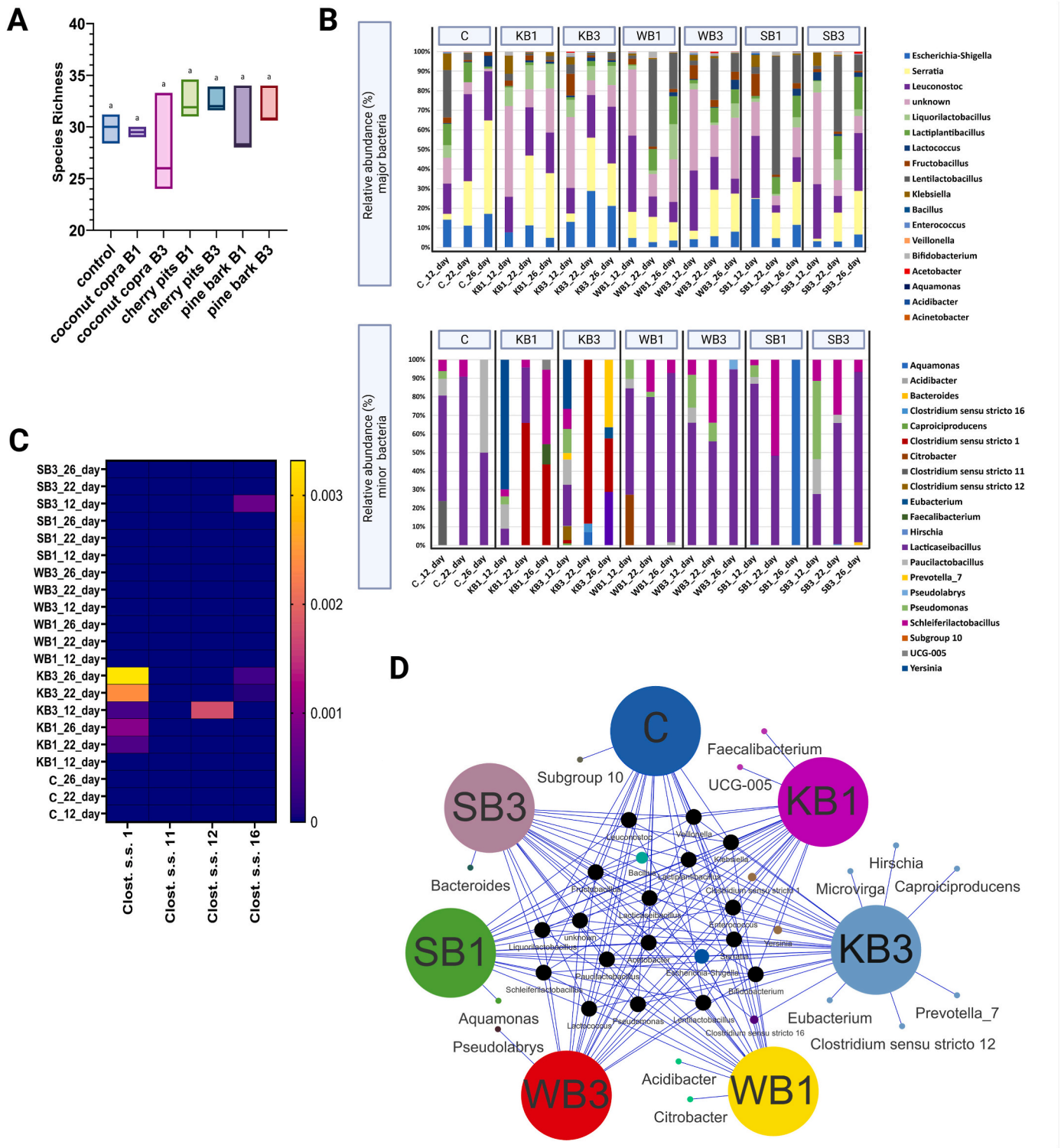

Fig. 5. Effects of biochar and sampling time point on microbial diversity and composition in dark fermentation bioreactors: A. Boxplots showing species richness. Bars labeled with the same letter indicate no statistically significant difference in richness ($p > 0.05$); B. Stacked bar plots representing the relative abundance of major (upper panel) and minor (lower panel) bacterial genera at particular time points. C. Heatmap showing the relative abundance of specific *Clostridium sensu stricto* subgroups (1, 11, 12 and 16) across all samples. Abundance is color-coded from low (blue) to high (yellow). D. Co-occurrence network of microbial genera showing relationships among bacterial taxa and their association with biochar types. Nodes represent genera and edges represent significant co-occurrence correlations. Reactor groups are color-coded. (For interpretation of the references to color in this figure legend, the reader is referred to the Web version of this article.)

the genus *Klebsiella*, belonging to the *Enterobacteriaceae* family, include species known to produce biohydrogen, such as *K. oxytoca*. Biohydrogen production by these bacteria occurs via the *Enterobacter*-type fermentation pathway [54].

Liquorilactobacillus belongs to the family *Lactobacillaceae*. Its correlation with increased biohydrogen production efficiency suggests that this taxon is involved in cross-feeding interactions that promote the production of hydrogen.

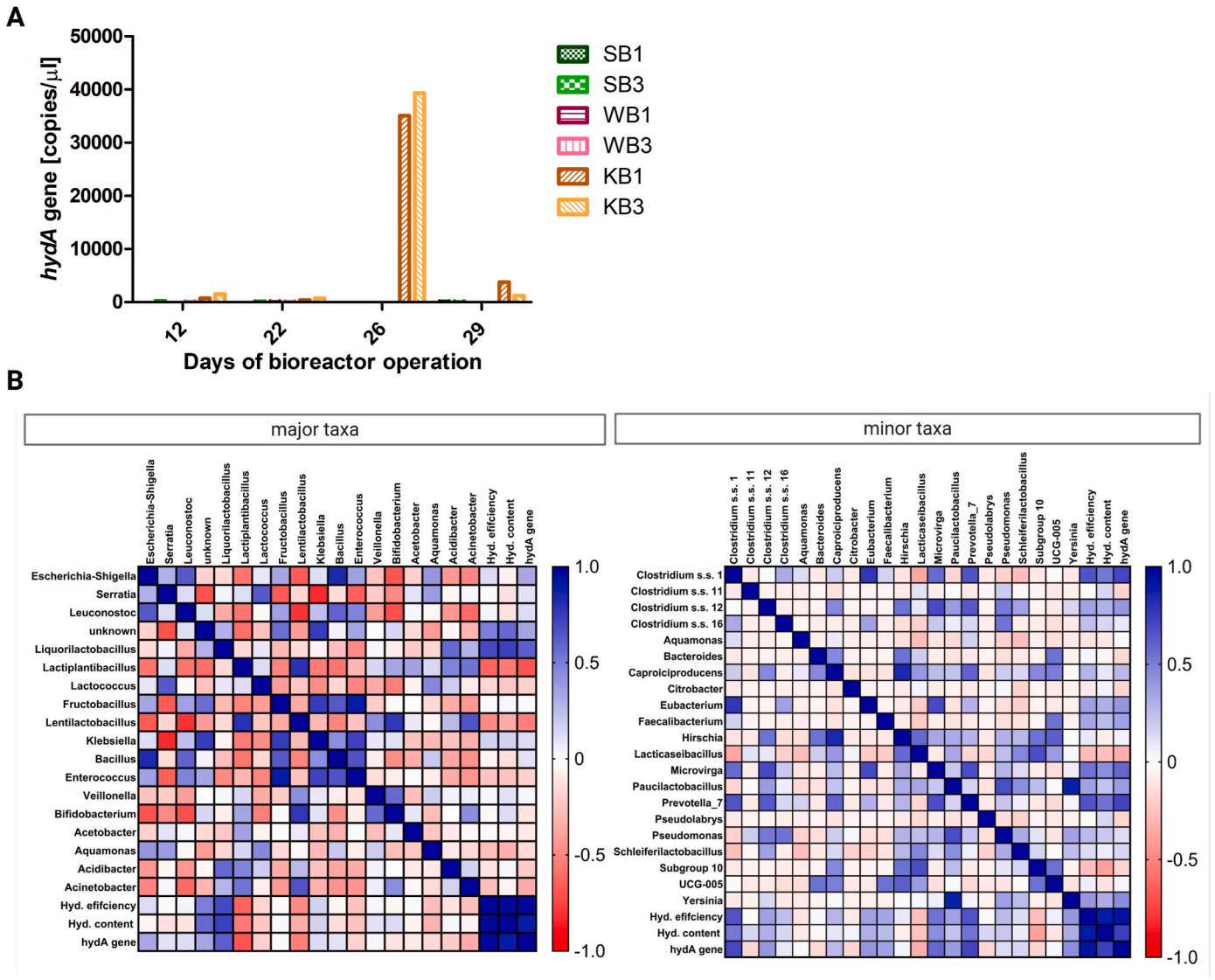

Fig. 6. Effects of biochar on the biohydrogen production potential of dark fermentation microbial communities. A. Average copy numbers of the *hydA* gene based on dPCR analysis of growth sampled from continuous operation phases 1 (day 12) and 3 (days 22, 26 and 29) of stage I. Each *hydA* gene copy number value is based on two determinations. B. Correlation analysis of microbial genera and biohydrogen production parameters: abundance of the *hydA* gene, biohydrogen production efficiency and biohydrogen content. The left heatmap presents major bacterial genera; the right heatmap, minor genera.

The heatmap shown in Fig. 6B indicates that the addition of coconut-derived biochar leads to the formation of an intermediate state in the bioreactors, positioned between a poorly performing control reactor and one approaching, but not attaining, optimal performance. This transitional state is comparable to that observed in batch experiments in our previous study (experiment ML), where lactate is the dominant fermentation product, butyrate production increases, and the contribution of *Clostridium* within the microbial communities rises [44]. A similar state was also identified in the continuous operation of the bioreactor PBR5 in a separate study [34].

In summary, biochar seems to induce a metabolic shift towards the equilibrium described in our previous studies [34,49], between lactic acid bacteria and biohydrogen producers. It is likely that this occurs through the enhancement of extracellular electron transfer by biochar, a phenomenon highlighted by others [13,16,20,21].

3.5. Biochars as an additional surface for biofilm formation

In analyzing the impact of biochar on biohydrogen production in a long-term continuous system, we also focused on the aspect of bacterial biofilm formation. It is widely accepted that in dark fermentation bioreactors, packing materials are employed to facilitate the immobilization of bacterial cells, and biofilm and granule formation to enhance biohydrogen production [33,34,55]. Scanning electron micrographs of initial biochar structures and post-experimental biochar after recovery from bioreactors confirmed that biochar provides a surface for bacterial biofilm development (Fig. 7). Our results support the assumption that biochar increases and diversifies the surfaces available for biofilm development [16,56]. Depending on the raw material and preparation method, the surface areas of biochar are highly variable, which affects the structure of the biofilm. In this study, pine-derived biochar was the most porous, while coconut-derived biochar exhibited the lowest porosity.

However, the formation of biofilm may also explain the biochar exhaustion effect (discussed in Section 3.1), manifested as a decrease in biohydrogen production efficiency. The results of previous studies indicate that biochar serves as a valuable source of minerals for bacteria (which will be discussed in more detail in Section 3.6). Therefore, the excessive development of biofilm on the surface, formed predominantly by non-biohydrogen producers, acts as a barrier to the accessibility and/

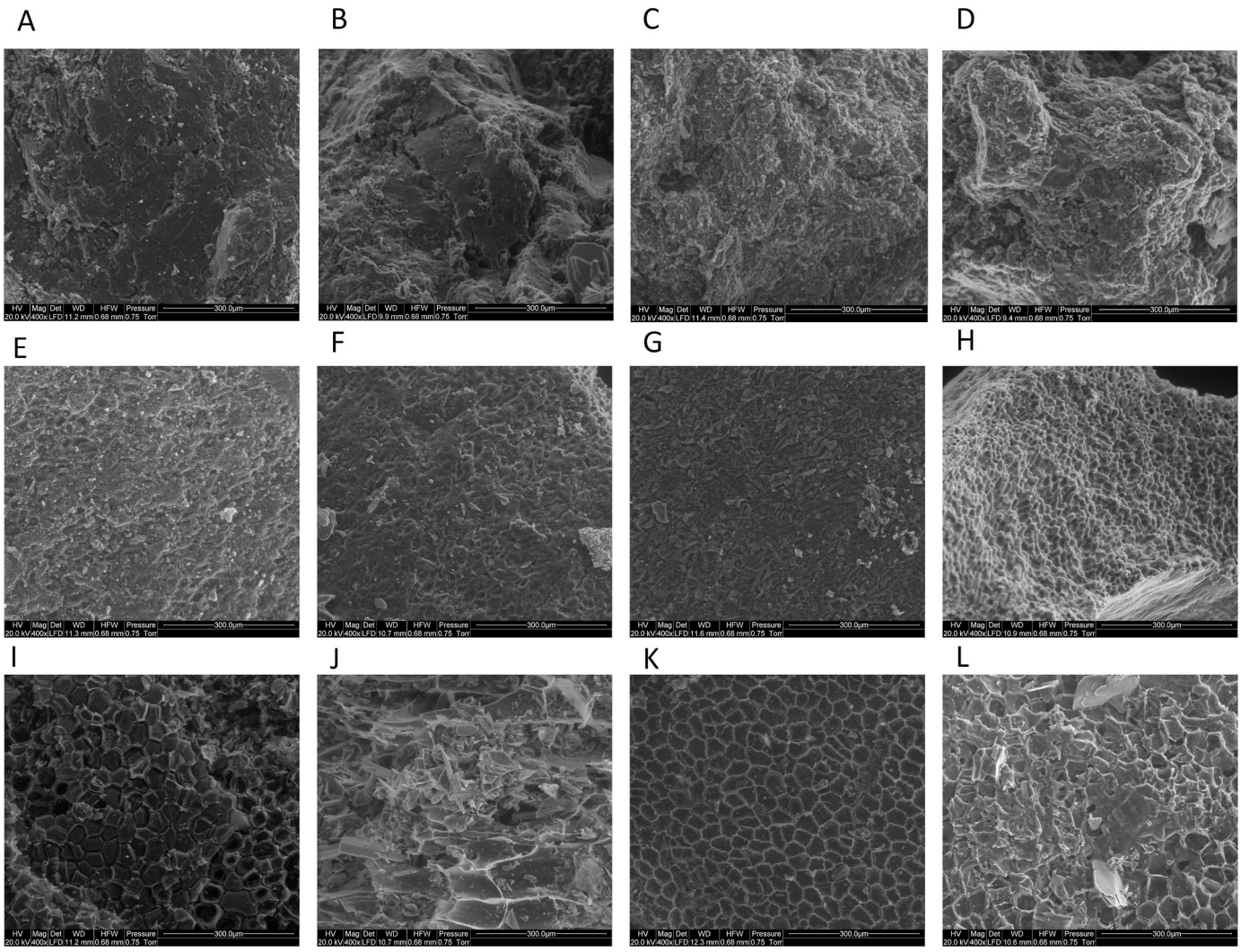

Fig. 7. Scanning electron micrographs of biochar surface structures (400× magnification): A, B – KB1; C, D – KB3; E, F – WB1; G, H – WB3; I, J – SB1; K, L – SB3. A, C, E, G, I, K – initial biochars before the experiment, B, D, F, H, J, L – post-experimental biochars.

or release of valuable elements for hydrogen-yielding bacteria. It is also possible that hydrogen-producing bacteria may be loosely associated with the biofilm or suspended in the bioreactor in the form of flocks or granules, and the removal of excess biomass from the bioreactor during renewal depletes the entire consortium to such an extent that it cannot regenerate to ensure efficient biohydrogen production, hence the need for reinoculation.

Our results indicate that in long-term continuous systems, unlike stationary ones, biofilm formation on biochar does not favor biohydrogen production. In general, excessive biomass growth is detrimental to biohydrogen generation, hence the need for periodic renewal and removal of biomass in continuous systems [33].

3.6. Elemental analysis of biochars and fermentation effluents

The positive effects of biochars on biohydrogen production stem directly from their unique properties. To identify these properties, and considering the widely accepted view that biochars serve as a mineral source for microorganisms [16,26], we analyzed the elemental composition of the tested biochars, both before addition to the bioreactors and after the completion of the experiment, both washed and unwashed. In addition, we performed elemental analysis on the fermentation effluents. Particular attention was paid to the properties of coconut copra biochar due to its distinctive ability to stimulate biohydrogen production. This analysis revealed that of the initial biochars, KB1 and KB3 are richer in elements other than carbon (Table 1), which is consistent with their 4-fold higher ash content compared to the WB and SB biochars (Section 2.1). Carbon constitutes approximately 80 % of the overall composition of coconut copra-derived biochar, whereas it accounts for 95 % of the WB and 96 % of the SB biochars. KB biochars also contain more nitrogen: around 7 %, compared to nearly 3 % in WB and <1 % in SB. Furthermore, they have higher levels of potassium (6–8 % vs. 0.8 % and 0.2 %), phosphorus (~2 % vs. 0.2 % and 0.04 %), and sulfur (0.2 % vs. >0.1 % and >0.05 %) when compared to WB and SB, respectively. Coconut copra biochar is also richer in minor elements (in the range of tenths to thousandths of a percent) such as sodium, magnesium, nickel, zinc and copper, but is poorer in calcium and aluminum.

In the analysis of the post-experimental biochar, we initially focused on comparing the elemental composition of the same type of biochar when covered with a bacterial biofilm (unwashed) and after the biofilm had been removed (washed) (Fig. 8, Supplementary Table 1). The following statistically significant differences in the levels of various elements were found: for KB1 regarding N, P, K and Cu; for KB3 regarding K, Mg and Ni; for SB1 and SB3 regarding P, K and Na. Apart from N, in all cases, the content of the aforementioned elements was always higher in the unwashed biochar, which indicates their accumulation in bacterial cells or biofilm structures. Similarly, comparison of the elemental composition of the initial biochar with the unwashed biochar, coated

Table 1
Elemental composition of initial biochars in mg/kg biochar and percentage contribution.

Element																			
biochar	C	N	S	P	K	Na	Ca	Mg	Fe	Al	Mn	Cu	Zn	Ni	Pb	Cr	V
KB1 [mg/kg]	633126	48998	1765	13311	44134	1374	1769	2164	207	40	147	90	131	14	1.1	3.3	0.30
[%]	84.72	6.56	0.24	1.78	5.91	0.18	0.24	0.29	0.03	0.005	0.020	0.012	0.018	0.0019	0.0001	0.0004	0.00004
KB3 [mg/kg]	689414	60213	2111	16261	71576	8932	1175	2135	1126	21	125	62	88	50	0.6	1.1	0.15
[%]	80.79	7.06	0.25	1.91	8.39	1.05	0.14	0.25	0.13	0.002	0.015	0.007	0.010	0.0059	0.0001	0.0001	0.00002
WB1 [mg/kg]	744075	22692	712	1719	6337	251	5669	1128	309	144	30	26	23	3	1.8	1.7	0.61
[%]	95.01	2.90	0.09	0.22	0.81	0.03	0.72	0.14	0.04	0.018	0.004	0.003	0.003	0.0004	0.0002	0.0002	0.0001
WB3 [mg/kg]	836190	22762	256	1749	6435	303	6107	1149	671	195	34	28	25	4	2.3	3.6	0.64
[%]	95.46	2.60	0.03	0.20	0.73	0.03	0.70	0.13	0.08	0.022	0.004	0.003	0.003	0.0005	0.0003	0.0004	0.0001
SB1 [mg/kg]	769850	6253	253	364	1914	483	12245	662	919	2353	331	8	41	4	7.6	4.0	1.80
[%]	96.75	0.79	0.03	0.05	0.24	0.06	1.54	0.08	0.12	0.296	0.042	0.001	0.005	0.0005	0.0010	0.0005	0.0002
SB3 [mg/kg]	802624	7229	200	344	1630	379	16276	598	915	963	383	8	55	5	6.3	6.8	1.50
[%]	96.51	0.87	0.02	0.04	0.20	0.05	1.96	0.07	0.11	0.116	0.046	0.001	0.007	0.0006	0.0008	0.0008	0.0002

with a bacterial biofilm, further confirmed this accumulation, except for K. Coconut copra-derived biochar seems to be a rich K source that bacteria probably utilize, since its concentration was several-fold lower in post-experimental KB biochars (KB1 and KB3). Post-experimental copra coconut-derived biochar was the richest source of elements (Fig. 8). In addition, it exhibited the property of persistent Mg accumulation, as evidenced by much higher concentrations of Mg in both washed and unwashed post-experimental biochar compared to the initial biochar. Pine bark-derived biochars, on the other hand, appear to be relatively rich in readily released iron, as indicated by comparison of the iron concentrations in the initial and post-experimental samples.

Many elements have a significant impact on biohydrogen production processes. This influence is dependent on their concentration; excessively low levels can lead to deficiencies, while excessively high levels can inhibit the process. The optimal concentration varies between elements and is determined by the type of substrate as well as the broader technical aspects of the process. Many elements, mainly metals, function as cofactors for enzymes that are involved in bacterial metabolism and cell growth. The impact on the catalyzed process is dependent on the relationship between cofactor concentration and enzymatic activity.

In our experimental setup, it does not appear that the nitrogen contained in biochar had any significant impact on biohydrogen production. It is a general rule that microorganisms utilize carbon 25–30 times faster than nitrogen during the anaerobic digestion of organic matter. Therefore, microbes require a C:N ratio of 20–30:1, with the majority of the carbon being readily degradable [57]. It is believed that this ratio should be even higher for efficient biohydrogen production at the acidogenesis stage during dark fermentation [58,59]. In the present study, regardless of the biochar employed, the C:N ratio of the fermented substrate was relatively low, which may have contributed to the significant instability of the process and the poor biohydrogen yield in the control bioreactor. In this setup, the situation would have worsened if additional N had been released from the biochar. Besides the C:N ratio, the C:P, C:N:P, and C:N:P:Fe ratios are also important [10]. P, present as phosphates, is involved in controlling redox potential, electron transfer between enzymatic complexes, and the reduction of Fd by NADH [8].

Fe, Ni and S form the active centers of hydrogenases, where iron-sulfur motifs are connected to Fe–Fe and Ni–Fe prosthetic groups, in [FeFe] and [NiFe] hydrogenases, respectively. Ferredoxins, which are iron-sulfur proteins, contain only iron-sulfur centers [9,60]. Enhanced biohydrogen production in dark fermentation reactors was observed after adding sources of Fe and Ni [14,25,30,61,62]. In all of these studies, the effects were concentration-dependent; an excess of the particular elements inhibited the process. Notably, low concentrations of sulfide also had a positive impact on biohydrogen production. High sulfide concentrations (100–800 mg/L) can inhibit anaerobic microorganisms by entering the cells and disrupting protein and enzyme functions. However, a low sulfide concentration (25 mg/L) significantly enhanced biohydrogen production (54 % higher than the control), suggesting that an optimal amount of dissolved S^{2-} can boost microbial metabolism. Sulfur is also an essential macronutrient for fermentative bacteria [63].

Na plays an important role in the formation of reduced ferredoxin. The translocation of Na^+ ions across the bacterial cell membrane creates an electrochemical gradient that enhances the reduction of Fd_{ox} by NADH, leading to a higher concentration of Fd_{red} [9,64]. It is hypothesized that K may also play a crucial role in sustaining membrane potential, modulating intracellular pH, and facilitating enzymatic functions, all of which could contribute to enhanced biohydrogen production. In addition, it has been demonstrated that potassium ferrate(VI) boosts biohydrogen generation during the dark fermentation of organic waste by breaking down organic materials and increasing the concentration of soluble organic matter [65,66]. Ca promotes the formation of biofilms and granules that are beneficial for biohydrogen production [9,10]. However, the molasses-containing medium in our system seems to provide sufficient Ca. Notably, the most effective biochar from coconut

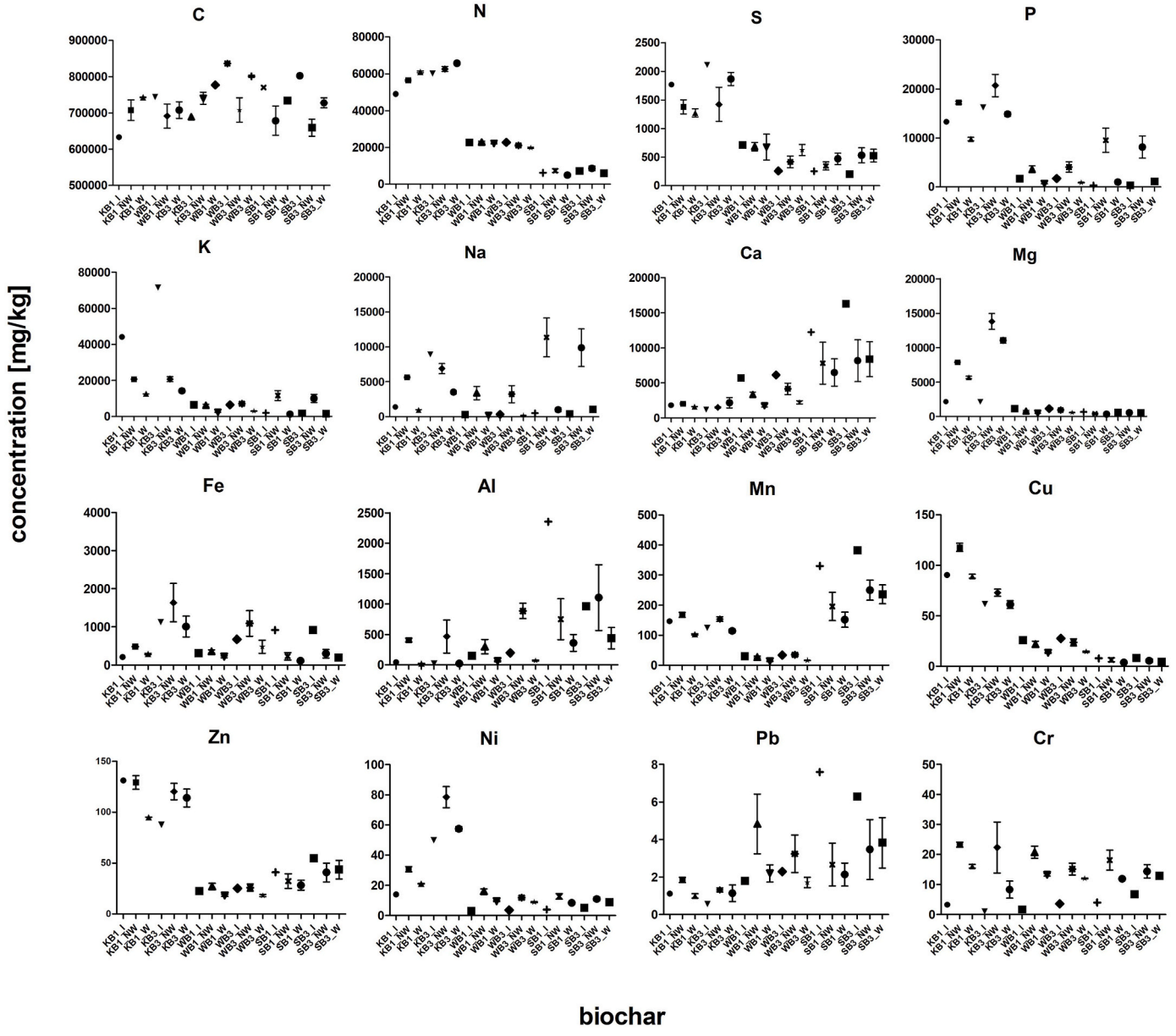

Fig. 8. Elemental composition of biochars: initial (I), post-experimental washed (W) and post-experimental unwashed (NW) samples. The whiskers extend to the SEM values, while the middle point indicates the mean value. Statistically significant differences (Tukey's Multiple Comparison Test) between washed and unwashed samples were observed for KB1 regarding N (*), P (*), K (**) and Cu (***); for KB3 regarding K (**), Mg (**) and Ni (***); for SB1 regarding P (**), K (***) and Na (***); for SB3 regarding P (*), K (**) and Na (***). *$p < 0.05$; **$p < 0.01$; ***$p < 0.001$.

copra contained the least amount of this element. As a cofactor of kinases and phosphatases, Mg is involved in glycolysis leading to pyruvate formation [9,10,67]. Poly-aluminum chloride has been shown to enhance biohydrogen production by inhibiting propionic acid fermentation and the activity of biohydrogen consumers during the dark fermentation of waste-activated sludge [68].

All biochars in our study tended to adsorb Cr. This indicates that biochars possess the property of absorbing toxic elements [16], which could lead to a specific type of "biochar toxicity" from the perspective of microbiological processes and potentially result in biochar exhaustion. Besides Cr, other elements known to inhibit biohydrogen production are Cu, Zn and Pb [9,10].

Elemental composition analysis of fermentation effluents did not reveal any statistically significant differences between the bioreactors. C was the most abundant element, followed by K, Na, P, N, S and Ca. The elements with the lowest concentrations in the bioreactor effluents were Cr, Ni, Cu and Pb. A similar percentage distribution was observed in the substrate containing sugar beet molasses supplied to the bioreactors. Since the percentage elemental composition in biochar and effluents differs, this indicates no significant release of elements from the biochar into the liquid phase in the bioreactors (Supplementary Fig. 2).

3.7. Principal Component Analysis

Principal component analysis (PCA) (Fig. 9) revealed that the first two principal components (PC1 and PC2) accounted for 39.4 % and 16.9 % of the total data variability, respectively, explaining a cumulative 56.3 % of the observed variation among the samples. The biplot indicated a clear separation of the KB1 and KB3 variants, which showed strong positive correlations with parameters such as P, S, N, the presence of the *hydA* gene, and biohydrogen production efficiency (Hyd. efficiency). In contrast, samples from the SB and WB variants exhibited

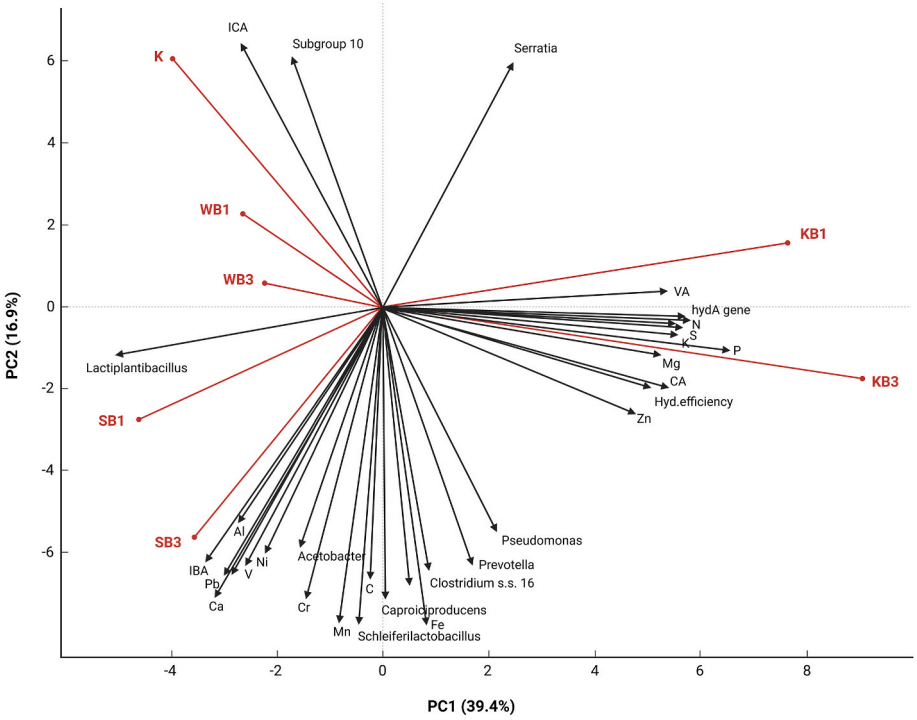

Fig. 9. Principal Component Analysis (PCA) performed on microbial communities, elemental composition, biohydrogen production efficiency, and *hydA* gene abundance. The score plot of PC1 (39.4 % variance) and PC2 (16.9 % variance) shows the degree of separation and similarity between the experimental variants; the accompanying loadings show the 30 parameters with the largest vector magnitudes contributing most to their differentiation.

distinct profiles associated with higher concentrations of elements such as Al, Ni, Cr and Pb, as well as with the bacterial genera *Acetobacter* and *Schleiferilactobacillus*. Overall, these results suggest that both the microbial composition and chemical parameters of the biochar play a crucial role in determining the efficiency of dark fermentation. Enrichment of hydrogen-producing microbial communities, particularly those harboring the *hydA* gene, is favored under nutrient-rich and metal-balanced conditions.

4. Conclusions

Of the materials added to the continuous dark fermentation bioreactors, coconut copra-derived biochar exhibits the most consistent and pronounced stimulatory effect, enhancing biohydrogen yields up to 15-fold (45 dm^3 H_2/kg COD molasses) compared with the control (2–3 dm^3 H_2/kg COD molasses). This improvement is associated with a 100-fold increase in *hydA* gene copies and selective enrichment of *Clostridium* sensu stricto subgroups 11, 12 and 1, as well as *Prevotella* and *Caproiciproducens*. The stimulatory effect is transient, requiring periodic biochar replacement and reinoculation with fresh inoculum to maintain stable biohydrogen production. This observation is particularly relevant because most previous studies have been limited to short-term batch systems, whereas industrial-scale implementation requires sustained performance under continuous operation.

Alkaline coconut copra biochar, enriched in potassium, phosphorus, sulfur, sodium, magnesium and nickel, promotes butyrate-type fermentation and enhances biohydrogen evolution, whereas mostly acidic pine bark and cherry pit biochars display weaker and unstable effects. Biochar does not contribute to pH changes in the acidic effluents, maintaining values in the mid-range of 4.2–4.6. Biochar origin and physicochemical characteristics, rather than pyrolysis conditions, determine microbial community composition and process outcomes. Continuous operation enables real-time assessment of microbial adaptation, biochar depletion, and system stability, revealing temporal dynamics that remain undetectable in batch assays.

Overall, this study advances the mechanistic understanding of biochar as both a microbial support surface and a nutrient reservoir, highlighting its feedstock-dependent efficacy and the critical importance of continuous systems for optimizing biochar application in sustainable biohydrogen production. Further studies aimed at maximizing the beneficial effects of biochars in such systems are warranted.

CRediT authorship contribution statement

Anna Detman-Ignatowska: Writing – review & editing, Writing – original draft, Visualization, Validation, Supervision, Resources, Project administration, Methodology, Investigation, Funding acquisition, Formal analysis, Data curation, Conceptualization. **Aleksandra Chojnacka:** Writing – review & editing, Visualization, Validation, Software, Methodology, Investigation, Formal analysis, Data curation, Conceptualization. **Martyna Paul:** Methodology, Investigation, Formal analysis, Data curation. **Gabriele Schiro:** Software, Methodology, Data curation. **Jerzy Jonczak:** Validation, Resources, Methodology, Investigation, Data curation. **Emilia Samborowska:** Validation, Resources, Methodology, Investigation, Data curation. **Jakub Karczmarski:** Validation, Resources, Methodology, Investigation, Data curation. **Anna Williams:** Methodology, Investigation, Data curation. **Daniel Laubitz:** Software, Resources, Methodology, Data curation. **Tadeusz Pęczek:** Validation, Methodology, Investigation, Data curation. **Karolina Drężek:** Visualization, Validation, Methodology. **Anna Sikora:** Writing – review & editing, Writing – original draft, Validation, Conceptualization.

Availability of data and materials

All data generated or analyzed during this study are included in this published article (and its supplementary information files). The raw DNA sequences generated in this study have been deposited in NCBI databases with the BioProject accession number PRJNA1291707, submission ID SUB15462781.

Funding sources

This work was supported by the National Science Centre, Poland, grant MINIATURA 5, UMO-2021/05/X/NZ9/00861.

Declaration of competing interest

The authors declare that they have no known competing financial interests or personal relationships that could have appeared to influence the work reported in this paper.

Acknowledgements

We would like to thank Dr. John Gittins for editorial assistance.

Appendix A. Supplementary data

Supplementary data to this article can be found online at https://doi.org/10.1016/j.ijhydene.2025.152812.

References

[1] Arizzi M, Morra S, Pugliese M, Gullino ML, Gilardi G, Valetti F. Biohydrogen and biomethane production sustained by untreated matrices and alternative application of compost waste. Waste Management 2016;56:151–7. https://doi.org/10.1016/j.wasman.2016.06.039.
[2] Bharathiraja B, Sudharsanaa T, Bharghavi A, Jayamuthunagai J, Praveenkumar R. Biohydrogen and biogas – an overview on feedstocks and enhancement process. Fuel 2016;185:810–28. https://doi.org/10.1016/j.fuel.2016.08.030.
[3] Fan Y, Zhang F, He K, Yu D, Chen H, Tian D, et al. Functional microorganisms in hydrogen production: mechanisms and applications. Bioresour Technol 2025;419:132007. https://doi.org/10.1016/j.biortech.2024.132007.
[4] Ghimire A, Frunzo L, Pirozzi F, Trably E, Escudie R, Lens PNL, et al. A review on dark fermentative biohydrogen production from organic biomass: process parameters and use of by-products. Appl Energy 2015;144:73–95. https://doi.org/10.1016/j.apenergy.2015.01.045.
[5] Jain R, Panwar NL, Jain SK, Gupta T, Agarwal C, Meena SS. Bio-hydrogen production through dark fermentation: an overview. Biomass Conv Bioref 2024;14:12699–724. https://doi.org/10.1007/s13399-022-03282-7.
[6] Khan MA, Ngo HH, Guo WS, Liu Y, Nghiem LD, Hai FI, et al. Optimization of process parameters for production of volatile fatty acid, biohydrogen and methane from anaerobic digestion. Bioresour Technol 2016;219:738–48. https://doi.org/10.1016/j.biortech.2016.08.073.
[7] Akiyama M, Osanai T. Regulation of organic acid and hydrogen production by NADH/NAD+ ratio in synechocystis sp. PCC 6803. Front Microbiol 2024;14:1332449. https://doi.org/10.3389/fmicb.2023.1332449.
[8] Atilano-Camino MM, Luévano-Montaño CD, García-González A, Olivo-Alanis DS, Álvarez-Valencia LH, García-Reyes RB. Evaluation of dissolved and immobilized redox mediators on dark fermentation: driving to hydrogen or solventogenic pathway. Bioresour Technol 2020;317:123981. https://doi.org/10.1016/j.biortech.2020.123981.
[9] Bundhoo MAZ, Mohee R. Inhibition of dark fermentative bio-hydrogen production: a review. Int J Hydrogen Energy 2016;41:6713–33. https://doi.org/10.1016/j.ijhydene.2016.03.057.
[10] Elbeshbishy E, Dhar BR, Nakhla G, Lee H-S. A critical review on inhibition of dark biohydrogen fermentation. Renew Sustain Energy Rev 2017;79:656–68. https://doi.org/10.1016/j.rser.2017.05.075.
[11] Hallenbeck PC. Fundamentals of the fermentative production of hydrogen. Water Sci Technol 2005;52:21–9. https://doi.org/10.2166/wst.2005.0494.
[12] Zhang J, Fan C, Zang L. Improvement of hydrogen production from glucose by ferrous iron and biochar. Bioresour Technol 2017;245:98–105. https://doi.org/10.1016/j.biortech.2017.08.198.
[13] Yang G, Wang J. Various additives for improving dark fermentative hydrogen production: a review. Renew Sustain Energy Rev 2018;95:130–46. https://doi.org/10.1016/j.rser.2018.07.029.
[14] Taherdanak M, Zilouei H, Karimi K. The effects of Fe0 and Ni0 nanoparticles versus Fe2+ and Ni2+ ions on dark hydrogen fermentation. Int J Hydrogen Energy 2016;41:167–73. https://doi.org/10.1016/j.ijhydene.2015.11.110.
[15] Wimonsong P, Nitisoravut R. Biohydrogen enhancement using highly porous activated carbon. Energy Fuels 2014;28:4554–9. https://doi.org/10.1021/ef500530v.
[16] Lou T, Yin Y, Wang J. Recent advances in effect of biochar on fermentative hydrogen production: performance and mechanisms. Int J Hydrogen Energy 2024;57:315–27. https://doi.org/10.1016/j.ijhydene.2024.01.039.
[17] Wang J, Wang S. Preparation, modification and environmental application of biochar: a review. J Clean Prod 2019;227:1002–22. https://doi.org/10.1016/j.jclepro.2019.04.282.
[18] Qiu L, Deng YF, Wang F, Davaritouchaee M, Yao YQ. A review on biochar-mediated anaerobic digestion with enhanced methane recovery. Renew Sustain Energy Rev 2019;115:109373. https://doi.org/10.1016/j.rser.2019.109373.
[19] Pan J, Ma J, Zhai L, Luo T, Mei Z, Liu H. Achievements of biochar application for enhanced anaerobic digestion: a review. Bioresour Technol 2019;292:122058. https://doi.org/10.1016/j.biortech.2019.122058.
[20] Li W, He L, Cheng C, Cao G, Ren N. Effects of biochar on ethanol-type and butyrate-type fermentative hydrogen productions. Bioresour Technol 2020;306:123088. https://doi.org/10.1016/j.biortech.2020.123088.
[21] Osman AI, Lai ZY, Farghali M, Yiin CL, Elgarahy AM, Hammad A, et al. Optimizing biomass pathways to bioenergy and biochar application in electricity generation, biodiesel production, and biohydrogen production. Environ Chem Lett 2023;21:2639–705. https://doi.org/10.1007/s10311-023-01613-2.
[22] Bu J, Wei H-L, Wang Y-T, Cheng J-R, Zhu M-J. Biochar boosts dark fermentative H2 production from sugarcane bagasse by selective enrichment/colonization of functional bacteria and enhancing extracellular electron transfer. Water Res 2021;202:117440. https://doi.org/10.1016/j.watres.2021.117440.
[23] Huang J-R, Chen X, Hu B-B, Cheng J-R, Zhu M-J. Bioaugmentation combined with biochar to enhance thermophilic hydrogen production from sugarcane bagasse. Bioresour Technol 2022;348:126790. https://doi.org/10.1016/j.biortech.2022.126790.
[24] Li W, Zhang Q, Cheng C, Xie Y, Liu M, Ren N, et al. Quantitative analysis of the mechanism of biochar in alleviating product inhibition in different fermentative hydrogen production processes. Biochar 2025;7:53. https://doi.org/10.1007/s42773-025-00453-3.
[25] Ramprakash B, Incharoensakdi A. Peanut shell activated carbon doped with nickel-iron nanoparticles as material for improving dark fermentative hydrogen production by Enterobacter aerogenes. Int J Hydrogen Energy 2025;99:579–88. https://doi.org/10.1016/j.ijhydene.2024.12.175.
[26] Sugiarto Y, Sunyoto NMS, Zhu M, Jones I, Zhang D. Effect of biochar in enhancing hydrogen production by mesophilic anaerobic digestion of food wastes: the role of minerals. Int J Hydrogen Energy 2021;46:3695–703. https://doi.org/10.1016/j.ijhydene.2020.10.256.
[27] Sun Y, Yang G, Zhang J, Wen C, Sun Z. Optimization and kinetic modeling of an enhanced bio-hydrogen fermentation with the addition of synergistic biochar and nickel nanoparticle. Int J Energy Res 2019;43:983–99. https://doi.org/10.1002/er.4342.
[28] Sunyoto NMS, Zhu M, Zhang Z, Zhang D. Effect of biochar addition on hydrogen and methane production in two-phase anaerobic digestion of aqueous carbohydrates food waste. Bioresour Technol 2016;219:29–36. https://doi.org/10.1016/j.biortech.2016.07.089.
[29] Yang G, Wang J. Synergistic enhancement of biohydrogen production from grass fermentation using biochar combined with zero-valent iron nanoparticles. Fuel 2019;251:420–7. https://doi.org/10.1016/j.fuel.2019.04.059.
[30] Yang Y, Bu J, Tiong YW, Xu S, Zhang J, He Y, et al. Enhanced thermophilic dark fermentation of hydrogen production from food waste by Fe-modified biochar. Environ Res 2024;244:117946. https://doi.org/10.1016/j.envres.2023.117946.
[31] Ying Z-Y, Zhang L-Y, Li Y, Wang Z-W, Qiao L, Wang F-H, et al. Effects of different types and pyrolysis temperature of straw biochar on promoting hydrogen production of sludge fermentation. Environmental Technology & Innovation 2025;37:104020. https://doi.org/10.1016/j.eti.2025.104020.
[32] Miller JH. Experiments in molecular genetics. Cold spring harbor. NY: Cold Spring Harbor Laboratory Press; 1972.
[33] Chojnacka A, Błaszczyk MK, Szczęsny P, Nowak K, Sumińska M, Tomczyk-Żak K, et al. Comparative analysis of hydrogen-producing bacterial biofilms and granular sludge formed in continuous cultures of fermentative bacteria. Bioresour Technol 2011;102:10057–64. https://doi.org/10.1016/j.biortech.2011.08.063.
[34] Detman A, Laubitz D, Chojnacka A, Wiktorowska-Sowa E, Piotrowski J, Salamon A, et al. Dynamics and complexity of dark fermentation microbial communities producing hydrogen from sugar beet molasses in continuously operating packed bed reactors. Front Microbiol 2021;11:612344. https://doi.org/10.3389/fmicb.2020.612344.
[35] Ostrowska J, Samborowska E, Jaworski M, Toczyłowska K, Szostak-Węgierek D. The potential role of SCFAs in modulating cardiometabolic risk by interacting with adiposity parameters and diet. Nutrients 2024;16:266. https://doi.org/10.3390/nu16020266.
[36] Pinu F, Villas-boas SG. Rapid quantification of major volatile metabolites in fermented food and beverages using gas chromatography-mass spectrometry. Metabolites 2017;7:37. https://doi.org/10.3390/metabo7030037.
[37] Sun S, Wang H, Xie J, Su Y. Simultaneous determination of rhamnose, xylitol, arabitol, fructose, glucose, inositol, sucrose, maltose in jujube (Zizyphus jujube Mill.) extract: comparison of HPLC–ELSD, LC–ESI–MS/MS and GC–MS. Chem Cent J 2016;10:25. https://doi.org/10.1186/s13065-016-0171-2.
[38] Caporaso JG, Lauber CL, Walters WA, Berg-Lyons D, Huntley J, Fierer N, et al. Ultra-high-throughput microbial community analysis on the Illumina HiSeq and MiSeq platforms. ISME J 2012;6:1621–4. https://doi.org/10.1038/ismej.2012.8.
[39] Wang Q, Garrity GM, Tiedje JM, Cole JR. Naïve bayesian classifier for rapid assignment of rRNA sequences into the new bacterial taxonomy. Appl Environ Microbiol 2007;73:5261–7. https://doi.org/10.1128/AEM.00062-07.
[40] Quast C, Pruesse E, Yilmaz P, Gerken J, Schweer T, Yarza P, et al. The SILVA ribosomal RNA gene database project: improved data processing and web-based tools. Nucleic Acids Res 2012;41:D590–6. https://doi.org/10.1093/nar/gks1219.
[41] Wang M-Y, Tsai Y-L, Olson BH, Chang J-S. Monitoring dark hydrogen fermentation performance of indigenous Clostridium butyricum by hydrogenase gene expression using RT-PCR and qPCR. Int J Hydrogen Energy 2008;33:4730–8. https://doi.org/10.1016/j.ijhydene.2008.06.048.

[42] D'Almeida AP, De Albuquerque TL. Coconut husk valorization: innovations in bioproducts and environmental sustainability. Biomass Conv Bioref 2024. https://doi.org/10.1007/s13399-024-06080-5.
[43] Mohd Jamaludin NF, Jamali NS, Abdullah LC, Idrus S, Engliman NS, Abdul PM. Biohydrogen production with utilisation of magnetite nanoparticles embedded in granular activated carbon from coconut shell. Int J Hydrogen Energy 2023;48:11695–708. https://doi.org/10.1016/j.ijhydene.2022.12.073.
[44] Detman A, Laubitz D, Chojnacka A, Kiela PR, Salamon A, Barberán A, et al. Dynamics of dark fermentation microbial communities in the light of lactate and butyrate production. Microbiome 2021;9:158. https://doi.org/10.1186/s40168-021-01105-x.
[45] García-Depraect O, Rene ER, Diaz-Cruces VF, León-Becerril E. Effect of process parameters on enhanced biohydrogen production from tequila vinasse via the lactate-acetate pathway. Bioresour Technol 2019;273:618–26. https://doi.org/10.1016/j.biortech.2018.11.056.
[46] García-Depraect O, Rene ER, Gómez-Romero J, López-López A, León-Becerril E. Enhanced biohydrogen production from the dark co-fermentation of tequila vinasse and nixtamalization wastewater: novel insights into ecological regulation by pH. Fuel 2019;253:159–66. https://doi.org/10.1016/j.fuel.2019.04.147.
[47] Detman A, Mielecki D, Chojnacka A, Salamon A, Błaszczyk MK, Sikora A. Cell factories converting lactate and acetate to butyrate: clostridium butyricum and microbial communities from dark fermentation bioreactors. Microb Cell Fact 2019;18:36. https://doi.org/10.1186/s12934-019-1085-1.
[48] Etchebehere C, Castelló E, Wenzel J, Del Pilar Anzola-Rojas M, Borzacconi L, Buitrón G, et al. Microbial communities from 20 different hydrogen-producing reactors studied by 454 pyrosequencing. Appl Microbiol Biotechnol 2016;100:3371–84. https://doi.org/10.1007/s00253-016-7325-y.
[49] Detman A, Laubitz D, Chojnacka A, Kiela PR, Salamon A, Barberán A, et al. Dynamics of dark fermentation microbial communities in the light of lactate and butyrate production. Microbiome 2021;9:158. https://doi.org/10.1186/s40168-021-01105-x.
[50] Díez MP, Villanueva-Galindo E, Moreno-Andrade I, Díaz E, De La Rubia MA, Mohedano AF, et al. Enhanced hydrogen production from food waste via bioaugmentation with clostridium and lactobacillus. Biomass Conv Bioref 2025. https://doi.org/10.1007/s13399-025-06628-z.
[51] Arizzi M, Morra S, Gilardi G, Pugliese M, Gullino ML, Valetti F. Improving sustainable hydrogen production from green waste: [fefe]-hydrogenases quantitative gene expression RT-qPCR analysis in presence of autochthonous consortia. Biotechnol Biofuels 2021;14:182. https://doi.org/10.1186/s13068-021-02028-3.
[52] De Sá LRV, De Oliveira TC, Dos Santos TF, Matos A, Cammarota MC, Oliveira EMM, et al. Hydrogenase activity monitoring in the fermentative hydrogen production using heat pretreated sludge: a useful approach to evaluate bacterial communities performance. Int J Hydrogen Energy 2011;36:7543–9. https://doi.org/10.1016/j.ijhydene.2011.03.119.
[53] Wang M-Y, Olson BH, Chang J-S. Relationship among growth parameters for Clostridium butyricum, hydA gene expression, and biohydrogen production in a sucrose-supplemented batch reactor. Appl Microbiol Biotechnol 2008;78:525–32. https://doi.org/10.1007/s00253-007-1317-x.
[54] Sikora A, Baszczyk M, Jurkowski M, Zielenkiewicz U. Lactic acid bacteria in hydrogen-producing consortia: on purpose or by coincidence? In: Kongo JM, editor. Lactic acid bacteria - r & D for food, health and livestock purposes. InTech; 2013. https://doi.org/10.5772/50364.
[55] Keskin T, Aksöyek E, Azbar N. Comparative analysis of thermophilic immobilized biohydrogen production using packed materials of ceramic ring and pumice stone. Int J Hydrogen Energy 2011;36:15160–7. https://doi.org/10.1016/j.ijhydene.2011.08.078.
[56] Lai SY. Emerging trend in porous carbon as catalysts support for biofuel production. Curr Opin Green Sustainable Chem 2025;52:101005. https://doi.org/10.1016/j.cogsc.2025.101005.
[57] Yadvika Santosh, Sreekrishnan TR, Kohli S, Rana V. Enhancement of biogas production from solid substrates using different techniques—a review. Bioresour Technol 2004;95:1–10. https://doi.org/10.1016/j.biortech.2004.02.010.
[58] Anzola-Rojas MDP, Gonçalves Da Fonseca S, Canedo Da Silva C, Maia De Oliveira V, Zaiat M. The use of the carbon/nitrogen ratio and specific organic loading rate as tools for improving biohydrogen production in fixed-bed reactors. Biotechnology Reports 2015;5:46–54. https://doi.org/10.1016/j.btre.2014.10.010.
[59] Lin C. Carbon/nitrogen-ratio effect on fermentative hydrogen production by mixed microflora. Int J Hydrogen Energy 2004;29:41–5. https://doi.org/10.1016/S0360-3199(03)00083-1.
[60] Calusinska M, Happe T, Joris B, Wilmotte A. The surprising diversity of clostridial hydrogenases: a comparative genomic perspective. Microbiology 2010;156:1575–88. https://doi.org/10.1099/mic.0.032771-0.
[61] Engliman NS, Abdul PM, Wu S-Y, Jahim JM. Influence of iron (II) oxide nanoparticle on biohydrogen production in thermophilic mixed fermentation. Int J Hydrogen Energy 2017;42:27482–93. https://doi.org/10.1016/j.ijhydene.2017.05.224.
[62] Wang J, Wan W. Influence of Ni2+ concentration on biohydrogen production. Bioresour Technol 2008;99:8864–8. https://doi.org/10.1016/j.biortech.2008.04.052.
[63] Dhar BR, Elbeshbishy E, Nakhla G. Influence of iron on sulfide inhibition in dark biohydrogen fermentation. Bioresour Technol 2012;126:123–30. https://doi.org/10.1016/j.biortech.2012.09.043.
[64] Westphal L, Wiechmann A, Baker J, Minton NP, Müller V. The rnf complex is an energy-coupled transhydrogenase essential to reversibly link cellular NADH and ferredoxin pools in the Acetogen Acetobacterium woodii. J Bacteriol 2018;200. https://doi.org/10.1128/JB.00357-18.
[65] Li X, Kuang Z, Zhang J, Liu X, Hu J, Xu Q, et al. Performance and mechanism of potassium Ferrate(VI) enhancing dark fermentative hydrogen accumulation from waste activated sludge. ACS Sustainable Chem Eng 2020;8:8681–91. https://doi.org/10.1021/acssuschemeng.0c01889.
[66] Yang J, Liu X, Liu X, Xu Q, Wang W, Wang D, et al. Enhanced dark fermentative hydrogen production from waste activated sludge by combining potassium ferrate with alkaline pretreatment. Sci Total Environ 2020;707:136105. https://doi.org/10.1016/j.scitotenv.2019.136105.
[67] Bao MD, Su HJ, Tan TW. Dark fermentative bio-hydrogen production: effects of substrate pre-treatment and addition of metal ions or L-cysteine. Fuel 2013;112:38–44. https://doi.org/10.1016/j.fuel.2013.04.063.
[68] Wu Y, Wang D, Liu X, Xu Q, Chen Y, Yang Q, et al. Effect of poly aluminum chloride on dark fermentative hydrogen accumulation from waste activated sludge. Water Res 2019;153:217–28. https://doi.org/10.1016/j.watres.2019.01.016.